Evolution of mechanical properties and final textural properties of resorcinol-formaldehyde xerogels during ambient air drying

A. Léonard[a], S. Blacher[a], M. Crine[a], W. Jomaa[b]

[a] Laboratory of Chemical Engineering, FNRS, University of Liège, Building B6c – Sart Tilman, 4000 Liège, Belgium

[b] TREFLE-ENSAM, UMR 8508, Esplanade des Arts et Métiers, 33405 Talence, France

Abstract

Porous carbon xerogels can be obtained by convective drying of resorcinol (*R*)-formaldehyde (*F*) hydrogels, followed by pyrolysis. Drying conditions have to be carefully controlled when crack-free monoliths with well-defined shape and size are required. The knowledge of the mechanical properties of the RF xerogels and their evolution with water content is essential to model their thermo-hygro-mechanical behaviour during convective drying and avoid mechanical stresses leading to deformation and cracking of the sample. The shrinkage behaviour and the mechanical properties of RF xerogels obtained with *R*/*C* ratio ranging from 300 to 1500 were investigated. *R*/*C* greatly influences the shrinkage and mechanical properties of the wet gel, on the one hand, and the mechanical and textural properties of the dried gel, on the other hand. The smaller the *R*/*C*, the higher the shrinkage, the stiffening, and the viscoelastic character of the xerogels. Water content has an influence on both the stiffness of the gels and the viscoelastic response. Generally, samples lose their mechanical viscous character and become more rigid when they are dried. Finally, mercury porosimetry measurements showed that the gels exhibit a marked lowering of

their stiffness upon compression, interpreted as a result of the heterogeneity of the microstructure.

PACS

81.05.Rm Porous materials; granular materials; 81.20.Fw Sol-gel processing, precipitation; 81.40.Jj Elasticity and anelasticity, stress-strain relations; 81.70.Bt Mechanical testing, impact tests, static and dynamic loads; 83.60.Bc Linear viscoelasticity;

1. Introduction

Production of carbon aerogels by CO_2 supercritical drying of resorcinol (*R*)-formaldehyde (*F*) hydrogels followed by pyrolysis in inert atmosphere has been extensively studied, since their introduction by Pekala [1] and [2]. RF hydrogels are usually synthesized using water as solvent and Na_2CO_3 (*C*) as pH regulator. The final texture of the material can be controlled by adjusting the *R*/*C* molar ratio. Supercritical conditions are used to preserve the pore texture, by avoiding surface tensions and shrinkage due to the appearance of liquid-vapour interfaces. With their large mesopore volumes (> 0.89 cm^3/g) and high specific surface areas (500-1200 m^2/g), potential applications of carbon aerogels are numerous: adsorbents for gas separation [3] and [4], catalysts supports [5], [6] and [7,7], electrode material for double layer capacitors [8], [9] and [10], energy storage device [11], column packing materials for chromatography,…

As supercritical drying remains difficult to apply at an industrial scale regarding its expensive and potentially dangerous character, other softer drying techniques have been tested in order to produce an aerogel-like mesoporous texture: freeze-drying [12],

vacuum drying [13], microwave drying [14], solvent exchange followed by freeze drying [15] or drying under nitrogen in tube furnace [16]. Some of us have shown recently that it is possible to produce porous resorcinol-formaldehyde xerogels by using atmospheric convective drying to remove the solvent, without any preliminary treatment [17]. Indeed, when synthesis conditions are adequate, the mechanical strength of the gel network is high enough to withstand capillary pressures, avoiding the collapse of the structure [18].

Monolithicity is one of the crucial properties of RF xerogels needed for many applications like electrodes or supercapacitors [10], [11], [19], [20] and [21]. For those applications a fixed shape and size of xerogels is required. In some cases, a sufficient mechanical strength is also required. To avoid cracking during the drying step [22], the knowledge of the evolution of the mechanical properties after curing is essential. Indeed, the simulation of the convective drying process by a coupled thermo-hygro-mechanical model requires the input of the mechanical properties and their evolution with water content [23] and [24].

After curing, resorcinol-formaldehyde materials cannot longer be qualified as gels as they are very stiff even if a lot of water is still present in the network (about 65% of the weight). In fact, these materials, that we will call xerogels, are viscoelastic materials that exhibit linear elastic behaviour under small strains and undergo densification and plastic hardening under high strains.

Beam-bending and shear velocity measurements were used to characterise either the wet gels, before [25] or after the curing step [26], or the aerogels obtained after supercritical drying [26]. All these measurements were performed on gels obtained with R/C ratio ranging between 50 and 200. Relaxation appeared to be mainly controlled by hydrodynamic phenomena, i.e. flow of water. The contribution of the network remains

low, except at low *R*/*C* ratio. Sound propagation experiments showed a decrease of RF aerogel stiffness when the samples are uniaxially compressed [27]. Recently, the same behaviour was found when RF samples are submitted to mercury porosimetry [28]. Gross et al. [26] showed that the elastic modulus is a power low function of density, over a limited range. They also found that the shear modulus increases by a factor up to 5 during supercritical drying. The same type of conclusions was obtained by Bock et al [29].

Mercury porosimetry, which is usually used to determine the pore size distribution [30] and [31], is affected by a peculiar behaviour in the case of RF samples [13], [17] and [28]. For this material, the pore size distribution cannot be obtained in a straightforward manner due to the collapse of the sample under mercury pressure [32]. Nevertheless the data allow to determine the compression modulus of the network according to Scherer's methodology [33]. This parameter has been shown to be related to the microstructure [28].

In this work, the evolution of mechanical properties of RF xerogels (elastic modulus, relaxation behaviour) with the residual water content is studied through uniaxial compression-relaxation tests performed in a standard traction-compression machine. Different levels of water contents are reached by drying the samples in ambient air, without any forced circulation. Stress relaxation data are interpreted using the Maxwell model or a generalised Maxwell model, as commonly applied for various materials [34], [35], [36], [37], [38] and [39].

Analysis of mercury porosimetry curves are performed in term of bulk modulus, in order to obtain information about the plastic hardening behaviour of these xerogels. The Poisson ratio at the dried state is determined by combining the results obtained by mercury porosimetry and uniaxial compression.

Finally N_2 adsorption-desorption measurements are used to link the obtained mechanical behaviour to the final texture of the xerogels. The influence of R/C ratio is investigated in a range between 300 and 1500, which is somewhat higher than value commonly reported in the literature.

2. Experimental

2.1. Sample preparation

Hydrogels were obtained by polycondensation of resorcinol (1,3-dihydroxybenzene) and formaldehyde in the presence of a Na_2CO_3, usually called catalyst (*C*). However, sodium carbonate does not really act as a catalyst but essentially modify the ratio OH^- /H^+. As these two species have an influence on the two steps constituting the polymerization mechanism [13], varying the *R*/*C* ratio modifies the final texture of the material [40].

For the preparation of hydrogels, 17.34 g of resorcinol (Vel, 99%) were first dissolved in 32.9 ml of deionised water under magnetic stirring, with the addition of Na_2CO_3 to achieve several *R*/*C* ratios (300, 600, 750, 900, 1200, 1500). After dissolution, 23.63 ml of formaldehyde solution (Aldrich, 37% wt. in water, stabilized by 10–15% wt. methanol) was added. The resorcinol/formaldehyde molar ratio *R*/*F* was fixed at 0.5 (stoichiometric ratio). Cylindrical samples were obtained by casting 5 ml solution into glass moulds (∅ = 22 mm) and putting them for curing under saturated atmosphere in an oven at 90°C during 24 h. Forced convection in the oven allowed high level of heat transfer during gelation. After gelation, the initial water content was determined according to standard methods [41]. For all the samples, the initial water content expressed on a dry basis, *W*, was close to 2 kg/kg.

2.2. Mechanical characterization

An Adamel Lhomargy DY-36 instrument (Paris, France), equipped with a 1 kN load cell, was used to determine the Young modulus of the gels by compressive axial loading of the cylindrical samples and simultaneous measurement of corresponding deformation. The gels were charged up to 700 N with a load rate of 0.5 N/s. Mechanical tests were performed on samples at different levels of humidity, obtained by ambient drying of the samples between two tests. This procedure ensured a uniform desiccation of the sample in order to limit internal moisture gradients. As the gelation is totally completed, only water is removed, and the samples remain in a monolithic shape. Young modulus, *E*, is the slope of the linear part of the plot of compressive stress versus strain. Stress is obtained by dividing the compressive load by the cross-sectional area, determined from the measurement of the diameter before each test. Strain is the change per unit length of the thickness of the sample. Two replicates were used for each *R*/*C* ratio.

Just after compression, the viscoelastic behaviour was evaluated through relaxation measurements during 2000 s. The stress-strain relationship for linear viscoelastic materials is given by the convolution product between the relaxation function $R(t)$ and the time derivative of viscoelastic strain (Eq. 1). The generalized Maxwell model is frequently used to model the relaxation function (Eq. 2). This model contains n Maxwell elements and an independent spring of elasticity modulus R_0 in parallel. A Maxwell element is constituted from a Hookean spring of elasticity modulus R_i, in series with a Newtonian dashpot of viscosity η_i. The relaxation time associated with each Maxwell element, defined as $\tau_i = \frac{\eta_i}{R_i}$, characterises the rate of decay of the stress in this element. One should define the main relaxation time as the one associated with the more significant Maxwell element.

$$\underline{\underline{\sigma}}(t) = R(t) \otimes \frac{\partial \underline{\underline{\varepsilon}}(t)}{\partial t} = \int_0^t R(t-\tau) \left. \frac{\partial \underline{\underline{\varepsilon}}}{\partial t} \right|_\tau d\tau \qquad \text{Eq. 1}$$

$$R(t) = R_0 + \sum_{i=1}^{n} \left\{ R_i \exp\left(-\frac{R_i}{\eta_i} t \right) \right\} = R_0 + \sum_{i=1}^{n} \left\{ R_i \exp\left(-\frac{t}{\tau_i} \right) \right\} \qquad \text{Eq. 2}$$

For uniaxial compression tests, the relaxation function $R(t)$ is the temporal evolution of the stress divided by the maximal strain obtained at the end of the compression stage. Moreover, the instantaneous modulus, which can be considered as the Young modulus determined during the compression test, is equal to the sum of all the elasticity modulus (Eq 3). Indeed, if a Dirac-type strain is applied, the generalized Maxwell model comes to a purely elastic model.

$$E = R_0 + \sum_{i=1}^{n} R_i \qquad \text{Eq. 3}$$

The ratio R_i/E reflects the importance of a Maxwell element in the mechanical behaviour of the material. When this ratio becomes less than 1%, the Maxwell element is not considered.

2.3. Mercury porosimetry and pycnometry

Mercury porosimetry measurements were made using a porosimeter Carlo Erba 2000 (CE Instruments, formerly Carlo Erba, UK). They were performed between 0.01 and 200 MPa, giving access to the volume of pores larger than 7.5 nm.

The apparent densities ρ_s of the samples were derived from mercury pycnometry. The geometrical volume of the sample is determined from the weight difference between a flask (calibrated volume) filled up with mercury and the same flask filled up with the sample and mercury. As mercury is a non-wetting liquid and as no pressure is exerted, mercury does not enter in the porosity of the sample or crush it. The intrinsic density of the dried xerogel, ρ_s^s, was measured with a helium pycnometer Accupyc 1330 (Micromeritics Inst. Co., USA).

2.4. Nitrogen adsorption desorption

Nitrogen adsorption isotherms measurements have been performed at 77 K on a "Micrometrics ASAP 2010M" (Micrometrics Inst. Co., USA) and on a "Fisons Sorptomatic 1990" (Fisons Instruments, UK). Each isotherm point is acquired when the pressure variation, within a fixed time, is lower than a fixed pressure deviation.

3. Results

3.1. Shrinkage behaviour

Size measurements were performed in order to determine the natural shrinkage of samples, i.e., when they are slowly dried at ambient temperature, without any air circulation. The resulting shrinkage curves, i.e. the sample volume divided by its initial value vs. the water content expressed on dry basis, obtained for the different R/C ratios are presented in Fig. 1. These curves show that the extent of shrinkage increases with decreasing R/C. There is almost no shrinkage for R/C = 1500, while a final volume reduction of about 55% is achieved for R/C = 300. All the curves (except R/C = 1500) follow the same 'master curve' during the zone of ideal shrinkage (linear part), and finish by a plateau when shrinkage has stopped.

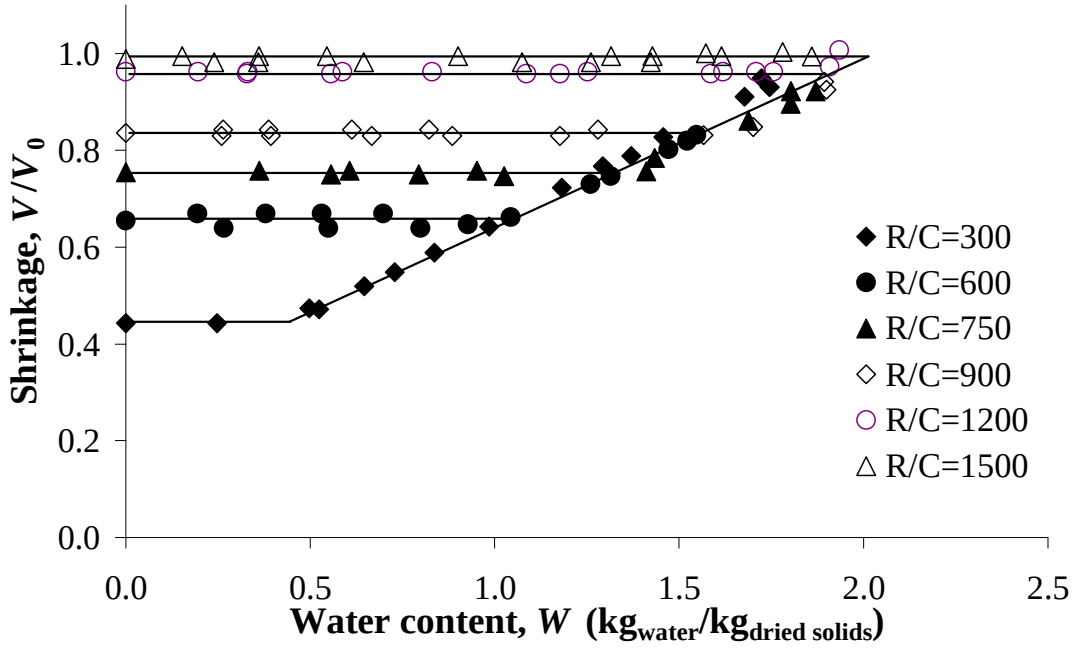

Fig. 1. Shrinkage curves – Each symbol represents the average of three measurements – The solid lines were drawn as guides to the eyes.

3.2 Mechanical properties

Typical compression curves obtained on samples prepared with *R*/*C*= 1500 and *R*/*C* = 300, i.e. extreme synthesis conditions, are presented in Fig. 2. For each sample, two curves are shown: one obtained just after removal from the mould, i.e. when the sample still contains a large quantity of water (~1.80 kg/kg), and a second at a lower water content (~0.65 kg/kg). Each trial presents a first curved phase corresponding to parallelism rectification and pre-consolidation of the sample followed by a linear part, corresponding to the elastic behaviour. Considering the slopes of the linear part, almost no evolution can be detected when *R*/*C* = 1500, while the rigidity of samples prepared with *R*/*C* = 300 increases with decreasing water content. This is confirmed by the evolution of Young modulus (*E*) vs. the water content for the different *R*/*C* ratios (Fig. 3 and Table 1). The Young modulus is almost independent of the water content for R/C =

1500 and 1200. For smaller *R*/*C*, it first increases with decreasing water content up to a maximum value above which it remains constant till complete dryness. The final rigidity of the dried sample increases with decreasing *R*/*C*.

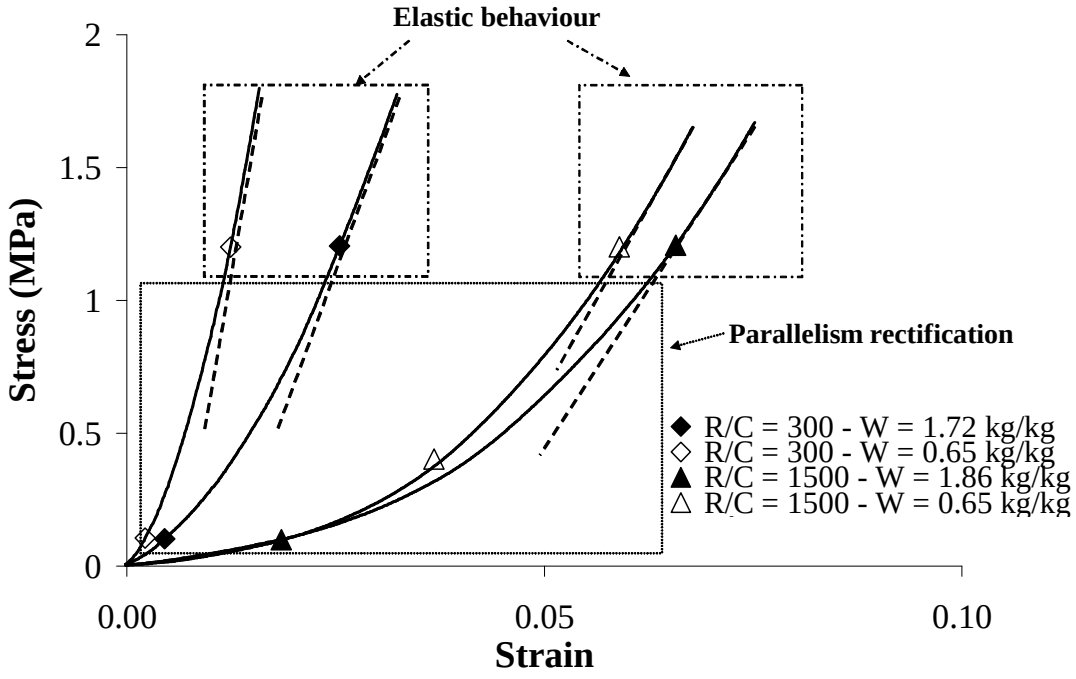

Fig. 2. Example of compression curves for samples prepared with *R*/*C*= 1500 and *R*/*C* 300. The solid lines follow the experimental points. Two symbols were added as labels on each data set. The dashed lines represent the tangent to the linear part from which the Young modulus was calculated.

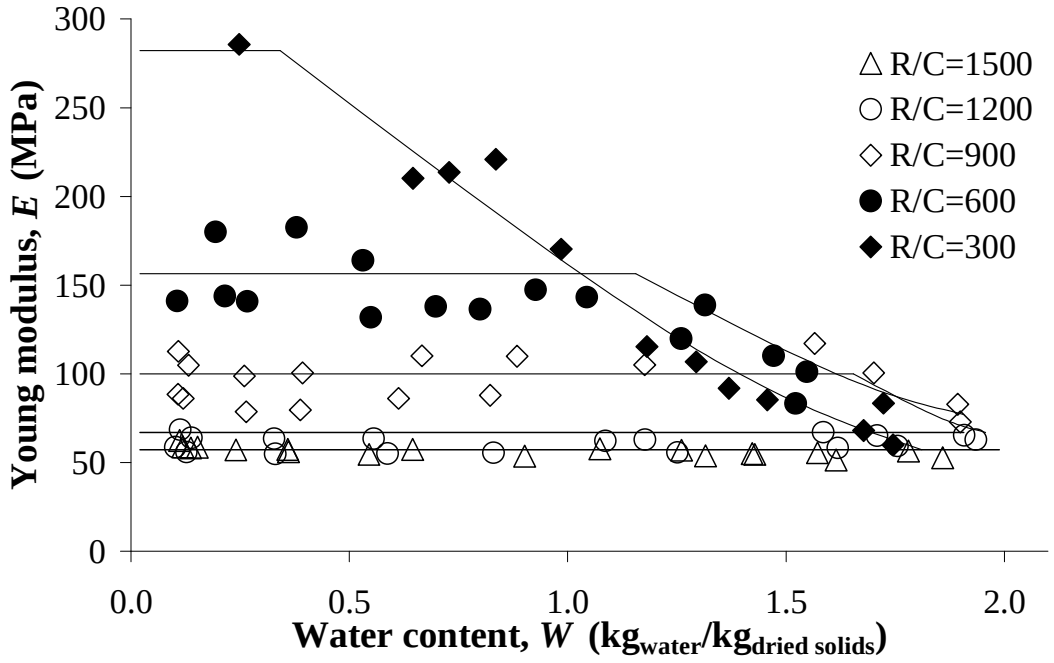

Fig. 3. Evolution of Young modulus with water content, for different *R*/*C* ratios; as results obtained for *R*/*C* = 750 are not significantly different from those related to *R*/*C* = 900, they are omitted for clarity. The curves through the data are guides for the eyes.

Relaxation experiments were performed in order to determine the viscoelastic behaviour of samples. Relaxation curves are illustrated in Fig. 4 for two synthesis conditions and two water contents. For *R*/*C* = 1500, the relaxation curves are nearly constant, which means samples are almost purely elastic. On the contrary, for *R*/*C* = 300, a relaxation phenomenon is clearly observed. It is characterized by a large decrease of *R*(*t*) with time. The effect of the residual water content is well marked for *R*/*C* = 1500: the viscous behaviour vanishes with increasing siccities. The relaxation functions obtained for the 6 different *R*/*C* ratios were modelled using the generalized Maxwell model (Eq. 2). According to our criteria, i.e. $R_i/E \geq 1\%$, Maxwell elements are sufficient to describe the viscoelastic behaviour the xerogels. Table 1 shows the parameters obtained by fitting, using a non-linear least squares method.

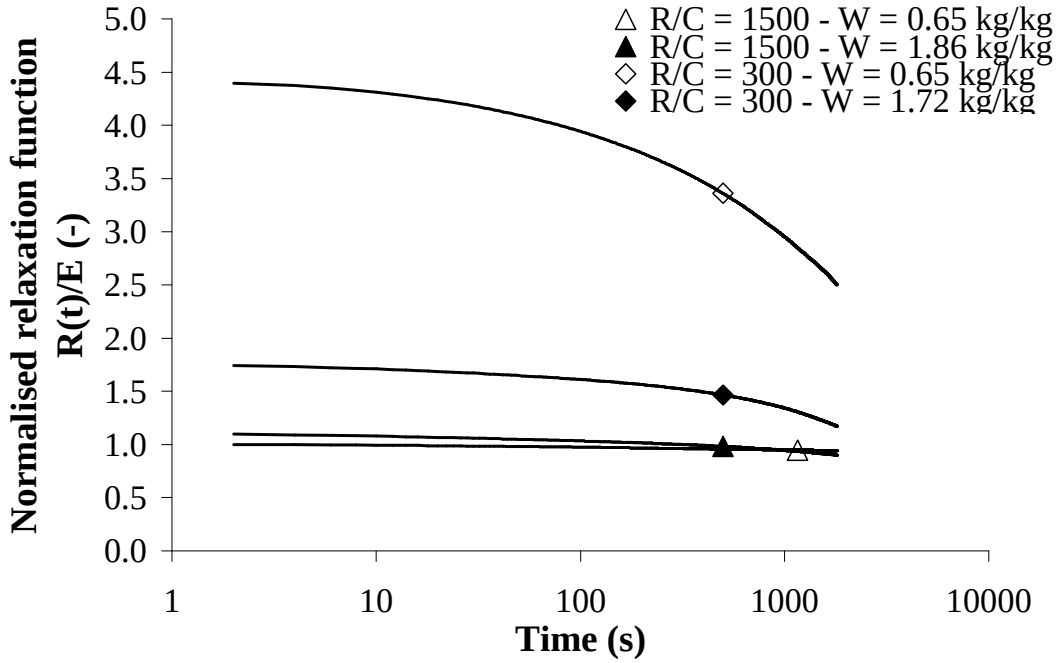

Fig. 4. Example of relaxation functions for samples prepared with *R*/*C*= 1500 and *R*/*C* 300. The solid lines follow the experimental points. One symbol was added as label on each data set.

Table 1.

Young modulus and fitting parameters of the generalized Maxwell model

R/C (-)	W (kg/kg) ± 0.01	R_0 (Mpa) ±1	R_1 (Mpa) ±1	τ_1 (s) ±10	R_2 (Mpa) ±1	τ_2 (s) ±50	R_0/E (%) ±4
1500	1.86	46	2	55	5	996	87
	1.57	49	2	52	5	990	89
	1.42	50	2	61	3	933	91
	1.26	52	2	60	3	914	91
	1.07	54	2	64	2	867	93
	0.65	51	1	60	2	877	89
	0.36	54	1	66	2	919	95
	0.24	53	1	57	3	869	93
	0.14	55	1	61	2	881	95
1200	1.91	50	1	20	13	1148	77
	1.71	53	2	31	10	1047	82
	1.59	57	2	44	7	1014	85
	1.18	57	2	56	4	981	90
	1.09	57	2	59	4	918	92
	0.56	60	1	67	3	854	94
	0.33	60	2	64	2	878	95
	0.14	59	1	59	3	963	92
	0.11	65	1	66	3	928	94
900	1.89	58	2	11	23	1130	70
	1.57	75	5	16	38	1169	64
	1.18	82	5	54	17	900	78
	0.88	99	3	71	8	838	90
	0.67	102	3	70	6	891	92
	0.39	93	3	75	4	771	93
	0.26	92	3	76	4	767	93
	0.13	97	2	71	6	969	92
	0.11	108	2	68	5	964	96
600	1.55	64	5	23	32	1083	63
	1.31	77	7	28	54	1384	55
	1.04	79	12	71	51	1033	55
	0.70	117	6	75	16	919	85
	0.53	152	5	87	9	824	93
	0.38	171	5	84	8	786	93
	0.19	174	2	67	6	995	97
	0.13	208	2	68	8	1017	97
300	1.72	52	4	15	29	1160	62
	1.46	53	4	16	30	1198	62
	1.37	58	5	24	29	1083	58
	1.18	69	8	45	39	995	60
	0.84	116	10	26	95	1175	52
	0.65	106	16	51	89	1081	50
	0.25	267	5	78	15	995	93

3.3. Textural properties of the dried gels

3.3.1. Mercury porosimetry

Mercury porosimetry curves obtained for all samples are presented in Fig. 5. Actually, the shape of these curves does not correspond to what is usually obtained with porous materials undergoing solely mercury intrusion. In the case of xerogels, an irreversible compression is observed in all the samples. On the curves, the compression region can be identified by a progressive increase of the mercury volume penetrating into the measurement cell. Intrusion seems only to arise for samples obtained with R/C = 1200 and R/C = 1500, as indicated by a sudden slope change at the end of the curves. The large hysteresis can be attributed to the fact that, when depressurization of the cell is realised, almost no mercury comes out of the sample, confirming its irreversible compression [42]. This peculiar behaviour of *RF* xerogels has been reported recently [32]. This hinders a straightforward textural interpretation of the mercury porosimetry curves. However these curves allow determining the total pore volume of samples, whose value can be related to the synthesis conditions. The specific pore volume measured (V_{Hg}, cm³/g) remains equal to the pore volume corresponding to pores larger than 7.5 nm. These results clearly show an evolution in the pore structure of the dried gels with R/C. The pore volume increases with R/C, suggesting that larger pore sizes are present (Table 2).

Because of this non usual behaviour during mercury porosimetry, it is possible to get information complementary to compressive uniaxial loading tests from the mechanical response of the dry material under the isostatic pressure. Since no mercury intrusion occurs, the compression modulus (K) can be related to the volume density (ϕ) according to Eq. 4., following to Scherer's methodology [33]. The volume density ϕ at the pressure of mercury P, defined as the ratio between the volume of the skeleton and the

total volume of the sample, can be expressed by Eq. 5. ρ_s^0 and ρ_s^s are the apparent density of the dried, uncompressed sample and the intrinsic density of the resin, measured by mercury and helium pycnometry, respectively (see Table 3).

$$K = \phi \frac{dP}{d\phi} \qquad \text{Eq. 4}$$

$$\phi(P) = \frac{1}{\rho_s^s \left(\frac{1}{\rho_s^0} - V_{Hg}(P) \right)} \qquad \text{Eq. 5}$$

The compression modulus (K) vs. the volume density (ϕ) is presented in Fig. 6 for the various R/C values. At low isostatic pressures (i.e. low density values), the compression modulus decreases abruptly, indicating that samples become softer. The compression modulus reaches then a minimum at values of ϕ (and P) which increase with decreasing R/C ratios. Beyond this minimum, K increases monotonously with ϕ (and P) for all the samples with R/C smaller than 1200, which indicates that crushing develops. For samples with largest R/C, i.e. 1200 and 1500, a second minimum is observed, which corresponds to the pressure at which intrusion begins.

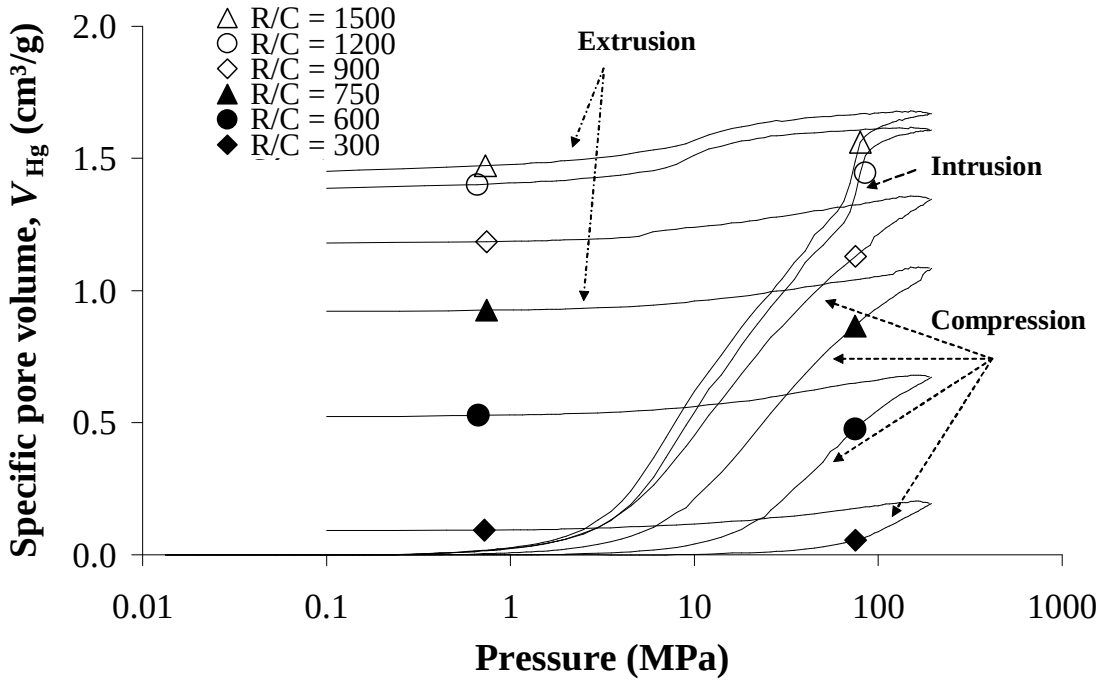

Fig. 5: Mercury porosimetry curves (volume variation as a function of mercury pressure). The solid lines follow the experimental points. Two symbols were added as labels on each data set.

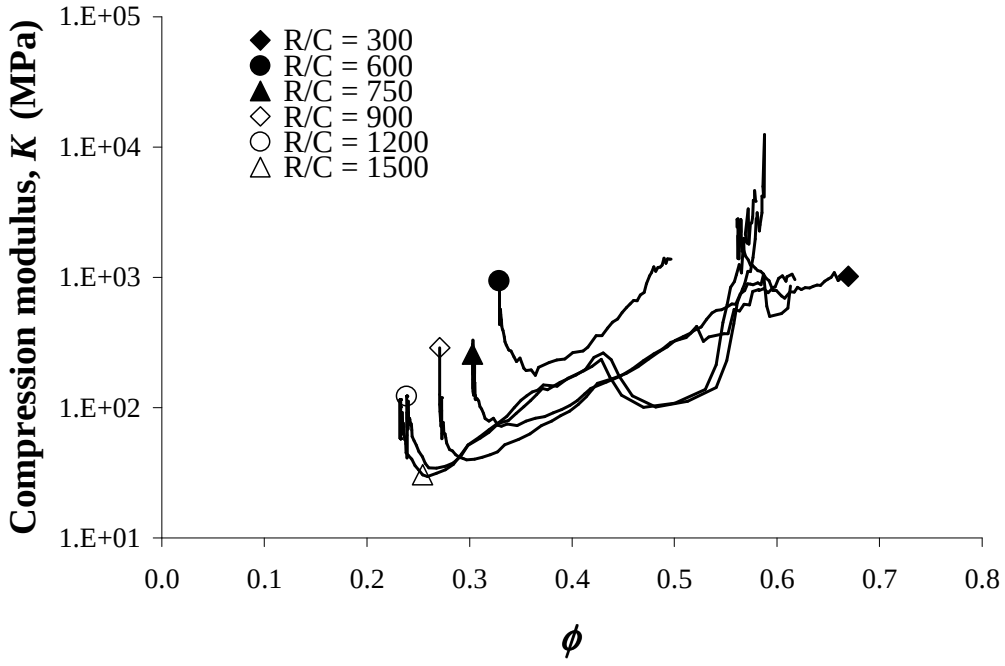

Fig. 6. Compression modulus K vs. ϕ. The solid lines follow the experimental points. One symbol was added as label on each data set

Combination of the results obtained from the mechanical compression tests, on the dried samples, and the mercury porosimetry measurements allows obtaining the Poisson ratio, υ, according to Eq. 6 [33]. Last column of Table 2 shows the values of the Poisson ratio corresponding to the dried state of the samples, i.e. taking into account the value of K and E obtained at the beginning of the mercury porosimetry measurements and at the end of the axial compression tests, respectively. The Poisson ratio ranges from 0.48 at low R/C to 0.42 at high R/C.

$$K = \frac{E}{3(1-2\upsilon)} \quad \text{Eq. 6}$$

3.3.2. Nitrogen adsorption-desorption

Nitrogen adsorption-desorption measurements carried out on dried gels are presented in Fig. 7. As R/C increases, xerogels evolve from micro-mesoporous texture for R/C = 300, (combination of type I at low p/p_0 and type II at high p/p_0 according to BDDT classification [43] to a micro-macroporous texture for higher R/C (combination of type I at low p/p_0 and type IV at high p/p_0). The shift of the hysteresis towards higher p/p_0 indicates that the mean pore size increases with R/C.

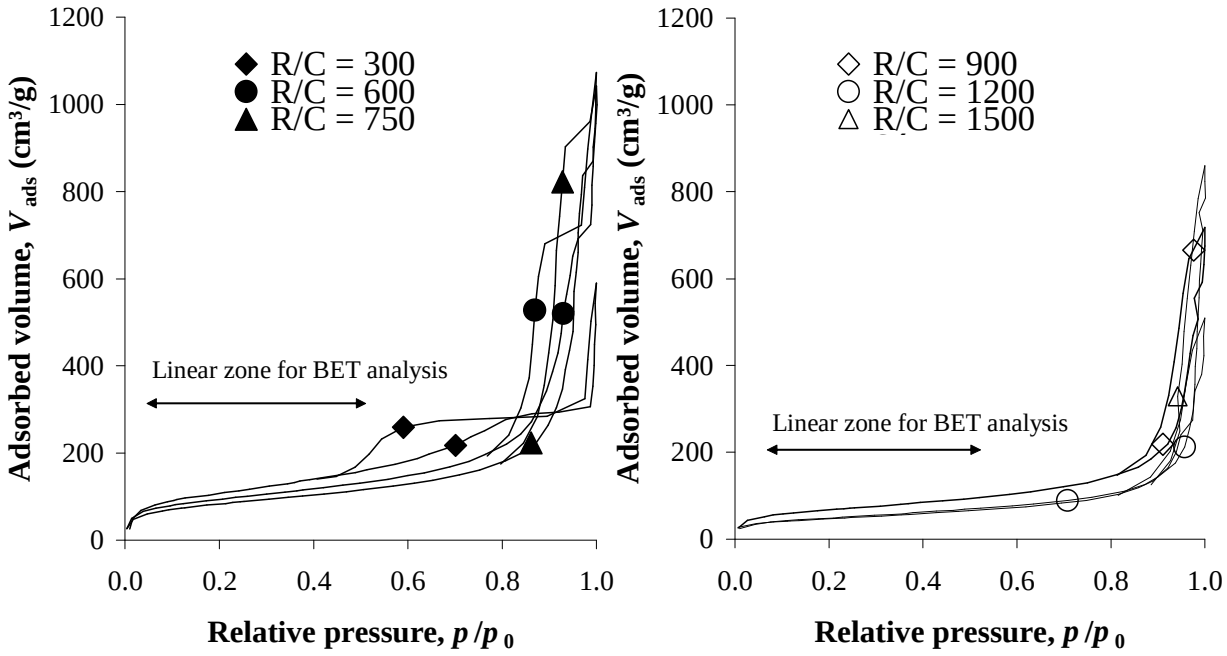

Fig.7. Nitrogen adsorption-desorption isotherms. The solid lines follow the experimental points. Two symbols were added as labels on each data set.

Table 2 shows that the specific surface area S_{BET} decreases with increasing *R*/*C*, and reaches a plateau for *R*/*C* = 1200 and *R*/*C* = 1500. Table 2 also indicates that the total porosity (ε), obtained from both apparent (ρ_s) and intrinsic (ρ_s^s) density measurements, increases with *R*/*C*.

Table 2.

Sample texture characterization

R/*C*	S_{BET} (m²/g) ± 5	V_{Hg} (cm³/g) ± 0.05	ρ_s (g/cm³) ±0.02	ρ_s^s (g/cm³) ±0.05	ε (%) ±0.01	ν (-) ±0.05
300	395	0.20	0.87	1.48	41	0.48
600	340	0.60	0.51	1.50	66	0.47
750	300	1.10	0.47	1.48	68	0.45
900	240	1.35	0.42	1.48	72	0.44
1200	170	1.60	0.37	1.45	75	0.42
1500	165	1.65	0.36	1.49	76	0.42

4. Discussion

In the case of ideal shrinkage, i.e. when the reduction of volume exactly corresponds to the volume of removed water, Eq. 7 can be applied to relate the volume (V) to the water content expresses on a dry basis (W). W_0 and ρ_w^w are the initial water content of the wet RF hydrogel, expressed on a dry basis, and the intrinsic density of water, i.e. 1000 kg/m³, respectively.

$$\frac{V}{V_0} = \left[\frac{1}{\frac{1}{\rho_s^s} + \frac{W_0}{\rho_w^w}} \right] \left[\frac{W}{\rho_w^w} + \frac{1}{\rho_s^s} \right] \qquad \text{Eq. 7}$$

The linear part of shrinkage curves observed on Fig. 1, and called ‘master curve’, indicates a zone of ideal shrinkage, whose extent differs according to the R/C ratio. During this period, no porosity is created. The theoretical value of the slope can be estimated from Eq. 7. One can found a value of 0.375, which is in agreement with the experimental one, 0.37 (see Fig. 1). The slope is the same for all the samples because they were prepared with the same dilution ratio, assuming the conversion degree of the polycondensation reaction was the same.

Concerning the elastic behaviour of the gels, their stiffening with decreasing water content can be directly related to the extent of shrinkage. Indeed, the increase of Young modulus is observed as long as xerogels undergo shrinkage. Once the shrinkage has stopped, no more stiffening of the network is observed. This indicates a clear relation between densification of the sample and elastic properties, as already reported by Woignier et al. [44] for silica aerogels. The Poisson ratios determined for the dried xerogels are of same order of magnitude as other polymers obtained by a condensation reaction, e.g. polyimides, polycarbonates, …

Regarding the viscoelastic behaviour of the gels, two Maxwell modules are required to fit the generalized Maxwell model (Eq. 2) on the relaxation curves. The associated relaxation times are close to 100 and 1000 s (see Table 1). One can notice that the main relaxation time is in the surroundings of 1000 s. It is rather difficult to assess whether this relaxation time corresponds to hydrodynamic or to network relaxation. Over the whole test series, the component R_0 represents the main contribution (more than 50%) to the relaxation function (see Table 1), which means elasticity prevails. Nevertheless, the extent of the elastic contribution depends on both the R/C ratio and the residual water content. For high moisture contents, the ratio R_0/E decreases with decreasing R/C, indicating more pronounced viscoelastic behaviour at low R/C. As already observed on Fig. 4, the samples obtained with R/C = 1500 are almost elastic and does not exhibit an important viscoelastic character. For a given R/C, R_0/E increases with decreasing water content, showing that the samples progressively lose their viscous character when water is removed. This last comment should authorize us to assess that the main relaxation mechanism should be related to the water migration during the relaxation period.

Shrinkage is favoured by high capillary forces, i.e. small pore sizes, and high mobility of the solid matrix. The mobility of the solid matrix is closely related to its physical state: high mobility corresponds to viscoelastic behaviour while low mobility corresponds to elastic behaviour [45]. The analysis of relaxation tests using the generalized Maxwell model showed that RF xerogels evolves from an almost purely elastic to pronounced viscoelastic behaviour as R/C decreases. Moreover, it is well admitted that the mean pore size inside the wet network decreases with decreasing R/C, resulting in polymeric RF gels at low R/C and colloidal gels at high R/C [40]. The combined effect of R/C on the mechanical behaviour and on the mean pore size of the humid network explains that higher volume reductions, and smaller pore sizes in the

dried state, are obtained for decreasing *R*/*C*. Consequently, the specific area obtained for the dried xerogels increases with decreasing *R*/*C*, as indicated by nitrogen adsorption-desorption results.

Finally, mercury porosimetry curves showed a peculiar behaviour in which stiffness first decreases with increasing pressure. This behaviour was firstly put in evidence by Gross et al [27] using the velocity of sound propagation on SiO_2 and RF aerogels for R/C=200. More recently, Gommes et al [28] reported similar results using mercury porosimetry measurements on RF xerogels with $5.8<pH<7.3$, which correspond roughly to $50<R/C<1200$ using mercury porosimetry measurements. They interpreted this behaviour as caused by the heterogeneity of the xerogel porous structure. When pressure is applied, the resulting load is shared among a small number of structures and the collapse is prevented by the surrounding smaller pores, in such a way that the reduction of volume is negligible. As a result, the macroscopic stiffness, *K*, decreases under the increasing pressure. After the minimum, the material undergoes a classical densification process. However, for samples obtained with $R/C = 1200$ and 1500, it seems that intrusion occurs at high pressure. That means that the stiffness of the network is sufficient to prevent any further collapse, and that there remain some mesopores. It is difficult to assess if these mesopores were initially present or if they result from the bulking of the structure, and the reduction in size of macropores.

5. Conclusions

In this paper, the shrinkage behaviour and the mechanical properties of RF xerogels obtained with *R*/*C* ratio ranging from 300 to 1500 have been investigated. All the results clearly showed the influence of the *R*/*C* ratio on the shrinkage and mechanical properties of the wet gel, on the one hand, and on the mechanical and textural properties

of the dried gel, on the other hand. Water content has an influence both on the stiffness of the gels and on the viscoelastic response. These results will be used in order to model the convective drying of RF xerogels, using a coupled hygro-thermo-mechanical model. The aim of this further work is to determine and minimize stress field and its evolution during drying, in order to avoid cracking of the samples.

Maxwell interpretation globalizes several mechanisms which are put in series but does not allow determining if the viscoelastic response corresponds mainly to the contribution of the solid skeleton, or of the liquid filling pores. Further work will be carried out using a model which will allow discrimination between the contribution of the liquid and the solid components to the viscoelasticity.

Acknowledgements

A. Léonard is grateful to the FNRS (National Fund for Scientific Research, Belgium) for a Postdoctoral Researcher position. A. Léonard also thanks the FNRS for supporting her scientific stay at the TREFLE Laboratory.

References

[1] R.W. Pekala, *J. Mater. Sci.* **24** (1989), p. 3221.

[2] R.W. Pekala and F.M. Kong, *Rev. Phys. Appl.* **24** (1989), p. 33.

[3] S. Sircar, T.C. Golden and M.B. Rao, *Carbon* **34** (1996), p. 1.

[4] T. Yamamoto, A. Endo, T. Ohmori and M. Nakaiwa, *Carbon* **42** (2004), p. 1671.

[5] M. Sanchez-Polo, J. Rivera-Utrilla and U. von Gunten, *Wat. Res.* **40** (2006), p. 3375.

[6] M.N. Padilla-Serrano, F.J. Maldonado-Hodar and C. Moreno-Castilla, *Appl. Catal. B-Environ.* **61** (2005), p. 253.

[7] C. Moreno-Castilla and F.J. Maldonado-Hodar, *Carbon* **43** (2005), p. 455.

[8] W. Li, G. Reichenauer and J. Fricke, *Carbon* **40** (2002), p. 2955.

[9] J. Li, X. Wang, Q. Huang, S. Gamboa and P.J. Sebastian, *J. Power Sources* **158** (2006), p. 784.

[10] R.W. Pekala, J.C. Farmer, C.T. Alviso, T.D. Tran, S.T. Mayer, J.M. Miller and B. Dunn, *J. Non-Cryst. Solids* **225** (1998), p. 74.

[11] E. Frackowiak and F. Beguin, *Carbon* **39** (2001), p. 937.

[12] B. Mathieu, S. Blacher, R. Pirard, J.P. Pirard, B. Sahouli and F. Brouers, *J. Non-Cryst. Solids* **212** (1997), p. 250.

[13] N. Job, R. Pirard, J. Marien and J.P. Pirard, *Carbon* **42** (2004), p. 619.

[14] T. Yamamoto, T. Nishimura, T. Suzuki and H. Tamon, *Dry. Technol.* **19** (2004), p. 1319.

[15] T. Yamamoto, T. Nishimura, T. Suzuki and H. Tamon, *Carbon* **39** (2001), p. 2374.

[16] C. Lin and J.A. Ritter, *Carbon* **35** (1997), p. 1271.

[17] A. Léonard, N. Job, S. Blacher, J.P. Pirard, M. Crine and W. Jomaa, *Carbon* **43** (2005), p. 1808.

[18] N. Job, F. Panariello, J. Marien, M. Crine, J.P. Pirard and A. Léonard, *J. Non-Cryst. Solids* **352** (2006), p. 24.

[19] S.W. Hwang and S.H. Hyun, *J. Non-Cryst. Solids* **347** (2004), p. 238.

[20] R. Saliger, U. Fischer, C. Herta and J. Fricke, *J. Non-Cryst. Solids* **225** (1998), p. 81.

[21] W. Li, H. Probstle and J. Fricke, *J. Non-Cryst. Solids* **325** (2003), p. 1.

[22] N. Job, F. Sabatier, J.P. Pirard, M. Crine and A. Léonard, *Carbon* **44** (2006), p. 2534.

[23] A. Léonard, M. Crine and W. Jomaa, in: I. Farkas (Ed.) *Proceeding of IDS 2006 - 15th International Drying Symposium,* **Vol. A** (2006), p. 273.

[24] F. Pourcel, W. Jomaa, J.R. Puiggali and L. Rouleau, *Powder Technol.* **172** (2006), p. 120.

[25] G.W.Scherer, C.T.Alviso, R.W.Pekala and J.Gross, in: R.F.Lobo, J.S.Beck, S.L.Suib, D.R.Corbin, M.E.Davis, L.E.Iton, and S.I.Zones (Eds.), *Microporous and Macroporous Materials*, Materials Research Society, (1996), p. 497.

[26] J. Gross, G.W. Scherer, C.T. Alviso and R.W. Pekala, *J. Non-Cryst. Solids* **211** (1997), p. 132.

[27] J. Gross, J. Fricke, R.W. Pekala and L.W. Hrubesh, *Phys. Rev. B* **45** (1992), p. 12774.

[28] C.J. Gommes, N. Job, S. Blacher and J.P. Pirard, *Studies in Surface Science and Catalysis* **160** (2006), p. 193.

[29] V. Bock, A. Emmerling and J. Fricke, *J. Non-Cryst. Solids* **225** (2005), p. 69.

[30] E.W. Washburn, *Proc. Nat. Acad. Sci.* (1921), p. 115.

[31] R. Pirard, S. Blacher, F. Brouers and J.P. Pirard, *J. Mater. Res.* **10** (1995), p. 2114.

[32] N. Job, R. Pirard, J.P. Pirard and C. Alie, *Part. Part. Syst. Charact.* **23** (2006), p. 72.

[33] G.W. Scherer, D.M. Smith, X. Qiu and J.M. Anderson, *J. Non-Cryst. Solids* **186** (1995), p. 316.

[34] J.F. Nicoleti, V. Silveira-Jr, J. Telis-Romero and V.R.N. Telis, *Lebensm. Wiss. Technol.* **38** (2005), p. 143.

[35] B.H. Hassan, A.M. Alhamdan and A.M. Elansari, *J. Food Eng.* **66** (2005), p. 439.

[36] J.L. Amoros, E. Sanchez, V. Cantavella and J.C. Jarque, *J. Eur. Ceram. Soc.* **23** (2003), p. 1839.

[37] N.C. Bertola, A.E. Bevilacqua and N.E. Zaritzky, *Lebensm. Wiss. Technol.* **28** (1995), p. 610.

[38] A.M. Herrero and M. Careche, *Food Res. Int.* **38** (2005), p. 69.

[39] F. Pourcel, PhD Thesis, Ecole Nationale Supérieure d'Arts et Métier, Bordeaux, France, 2003.

[40] S.A. Al Muhtaseb and J.A. Ritter, *Adv. Mater.* **15** (2003), p. 101.

[41] ASAE. American Society of Agricultural Engineers (Eds), *ASAE Standard n°D245.5*, St. Joseph, Michigan (1996), p. 452.

[42] R. Pirard, A. Rigacci, J.C. Marechal, D. Quenard, B. Chevalier, P. Achard and J.P. Pirard, *Polymer* **44** (2003), p. 4881.

[43] A.J.Lecloux, in: J.R.Anderson and M.Boudart (Eds.), *Catalysis: Science and Technology vol. 2*, Springer, Berlin, (1981), p. 171.

[44] T. Woignier, J. Reynes, A. Hafidi Alaoui, I. Beurroies and J. Phalippou, *J. Non-Cryst. Solids* **241** (1998), p. 45.

[45] L. Mayor and A.M. Sereno, *J. Food Eng.* **61** (2004), p. 373.

Figure captions

Fig. 1. Shrinkage curves - curves – Each symbol represents the average of three measurements – The solid lines were drawn as guides to the eyes.

Fig. 2. Example of compression curves for samples prepared with *R*/*C*= 1500 and *R*/*C* 300. The solid lines follow the experimental points. Two symbols were added as labels on each data set. The dashed lines represent the tangent to the linear part from which the Young modulus was calculated.

Fig. 3. Evolution of Young modulus with water content, for different *R*/*C* ratios; as results obtained for *R*/*C* = 750 are not significantly different from those related to *R*/*C* = 900, they are omitted for clarity. The curves through the data are guides for the eyes.

Fig. 4. Example of relaxation functions for samples prepared with *R*/*C*= 1500 and *R*/*C* 300. The solid lines follow the experimental points. One symbol was added as label on each data set.

Fig. 5. Mercury porosimetry curves (volume variation as a function of mercury pressure). The solid lines follow the experimental points. Two symbols were added as labels on each data set.

Fig. 6. Compression modulus K vs. ϕ. The solid lines follow the experimental points. One symbol was added as label on each data set.

Fig. 7. Nitrogen adsorption-desorption isotherms. The solid lines follow the experimental points. Two symbols were added as labels on each data set.

Tables

Table 1: Young modulus and fitting parameters of the generalized Maxwell model

Table 2: Sample texture characterization